Available online at www.sciencedirect.com
ScienceDirect
Applied Surface Science 253 (2006) 1274–1281
applied surface science
www.elsevier.com/locate/apsusc

Influence of surface energy and relative humidity on AFM nanomechanical contact stiffness☆

D.C. Hurley [a,*], M. Kopycinska-Müller [a], D. Julthongpiput [b], M.J. Fasolka [b]

[a] Materials Reliability Division, National Institute of Standards & Technology, 325 Broadway, Boulder, CO 80305-3328, USA
[b] Polymers Division, National Institute of Standards & Technology, 100 Bureau Drive, Gaithersburg, MD 20899-8542, USA

Received 22 November 2005; accepted 31 January 2006
Available online 9 March 2006

Abstract

The effects of surface functionality and relative humidity (RH) on nanomechanical contact stiffness were investigated using atomic force acoustic microscopy (AFAM), a contact scanned-probe microscopy (SPM) technique. Self-assembled monolayers (SAMs) with controlled surface energy were studied systematically in a controlled-humidity chamber. AFAM amplitude images of a micropatterned, graded-surface-energy SAM sample revealed that image contrast depended on both ambient humidity and surface energy. Quantitative AFAM point measurements indicated that the contact stiffness remained roughly constant for the hydrophobic SAM but increased monotonically for the hydrophilic SAM. To correct for this unphysical behavior, a viscoelastic damping term representing capillary forces between the tip and the SAM was added to the data analysis model. The contact stiffness calculated with this revised model remained constant with RH, while the damping term increased strongly with RH for the hydrophilic SAM. The observed behavior is consistent with previous studies of surface energy and RH behavior using AFM pull-off forces. Our results show that surface and environmental conditions can influence accurate measurements of nanomechanical properties with SPM methods such as AFAM.
Published by Elsevier B.V.

PACS: 62.25.+g; 68.37.Ps; 82.35.Gh

Keywords: Atomic force microscopy (AFM); Nanomechanics; Self-assembled monolayer (SAM)

1. Introduction

As applications for nanotechnology multiply, demand increases for new ways to characterize materials on commensurate scales. In particular, nanoscale information about mechanical properties is desired. Knowledge of mechanical properties is critical to successful development of thin-film and nanoscale assemblies, and to assess reliability in applications from microelectronics to biotechnology. Scanned-probe microscopy (SPM) methods involving the atomic force microscope (AFM) are an attractive tool for nanoscale characterization due to the small probe tip diameter ($\sim$10–100 nm), low applied loads ($\sim$0.01–10 μN), and scanning or imaging ability. Not surprisingly, several SPM methods for nanomechanical measurements have already been demonstrated. Atomic force acoustic microscopy (AFAM) [1] is one such emerging method that has been shown to provide quantitative elastic-property information. However, further research is needed on several issues that affect the accuracy and reliability of quantitative AFAM measurements.

Here we examine one such issue, namely the effect of the interplay of surface functionality and relative humidity (RH) on AFAM measurements of nanoscale contact stiffness. In many contact methods, the contact stiffness serves as the link between the measured quantities and the elastic modulus of the sample. In previous experiments on thin films of fluorosilicate glass [2], we observed that the apparent contact stiffness depended on the ambient humidity for one thin-film sample. Such variability presents a potential roadblock to measurement accuracy. Moreover, surface chemistry plays a significant role in many physical properties including thin-film behavior, adhesion and wetting, and friction. It is therefore important to understand its

☆ Contribution of NIST, an agency of the US government; not subject to copyright.

* Corresponding author. Tel.: +1 303 497 3081; fax: +1 303 497 5030.
E-mail address: hurley@boulder.nist.gov (D.C. Hurley).

0169-4332/$ – see front matter. Published by Elsevier B.V.
doi:10.1016/j.apsusc.2006.01.072

impact on contact SPM methods such as AFAM. In this work, we have performed further experiments under carefully controlled conditions to systematically investigate the effects of RH and surface energy. The experiments involved specimens containing self-assembled monolayers (SAMs) whose surface energy (relative hydrophobic/hydrophilic nature) could be adjusted [3,4]. The experiments were performed over a wide range of RH values in a controlled-humidity chamber for the AFM. These experiments have increased our understanding of the interaction between the SPM tip and the sample under a variety of conditions. This increased understanding improves our ability to accurately measure elastic properties on an extended range of materials.

2. Experimental methods

2.1. AFAM techniques

In simplest terms, AFAM involves exciting and detecting the resonant modes of an AFM cantilever beam. The resonant frequencies of the cantilever when its tip is in contact with a sample—the ''contact-resonance frequencies''—can be used to measure the elastic modulus of the sample. The experimental AFAM apparatus has been described in detail previously [1,5]. In summary, the sample is mounted on a piezoelectric actuator (commercial ultrasonic contact transducer). The actuator is excited by a continuous sine-wave voltage (frequency $\sim$0.1–3.5 MHz, root-mean-square amplitude $\sim$0.05–0.5 V). When the tip of the AFM cantilever is brought in contact with the sample at a static applied load F_c, the frequencies of the resonant modes increase from their free-space values due to tip–sample forces that stiffen the system. Here we consider only the two lowest flexural (bending) modes of the cantilever. To detect the amplitude of the cantilever vibration, the AFM photodiode signal is processed by a lock-in amplifier.

This AFAM apparatus can be used in two different ways: for *qualitative* amplitude images or for *quantitative* point measurements. To obtain AFAM amplitude images, the excitation frequency of the transducer is held constant at a value close to that of the contact-resonance frequency. The output amplitude signal of the lock-in amplifier is used as input to the AFM auxiliary image channel. In the resulting image, the intensity corresponds to the relative amplitude of the cantilever vibration at the excitation frequency. The contrast in AFAM amplitude images depends on the variation in cantilever vibration amplitude at different positions on the sample [6]. Image contrast can be enhanced by the choice of excitation frequency over a range that depends on the relative elastic properties of the different sample components or phases. In images acquired with an excitation frequency at the lower end of this range, the cantilever vibration amplitude will be higher for regions with lower elastic modulus. Thus, more compliant regions will appear brighter in the image. Increasing the excitation frequency until it is close to the contact-resonance frequency of stiffer sample components causes a decrease in the vibration amplitude of the more compliant regions. In these images, brighter areas correspond to stiffer sample components. Thus, we can observe a reversal or ''inversion'' in image contrast by changing the excitation frequency. This behavior means that different material components can be easily identified with AFAM amplitude images, but using them to evaluate the relative mechanical properties of each component is more complicated.

Quantitative modulus information can be obtained by a second AFAM approach involving spectral measurements. In this case, the cantilever tip remains in one place on the sample. The excitation frequency is repeatedly incremented by the computer, and the resulting output signal of the lock-in detector is recorded. In this way, spectra of the cantilever response versus frequency are obtained. The contact-resonance frequency spectra are interpreted with an analytical model for the cantilever beam dynamics. The model relates the measured frequencies to one or more parameters that characterize the tip–sample interaction, as shown in Fig. 1. The cantilever is represented by a rectangular beam of length L that is clamped at one end. The tip is located at a distance L_1 from the clamped end of the cantilever; the remaining distance to the unclamped end is L'. The simplest model to describe the tip–sample interaction is a spring of stiffness k^* between the tip and the sample, representing a purely elastic interaction. To include the effect of a viscoelastic damping interaction between the tip and the sample, a dashpot with characteristic damping σ in parallel with the spring can be added. Closed-form expressions that relate the contact-resonance frequencies to the contact stiffness for the case of a purely elastic interaction ($\sigma = 0$) [1] and for viscoelastic interaction ($\sigma \neq 0$) [2,7] have been published previously and are not reproduced here.

With the closed-form expressions, values of k^* (and σ) may be calculated from the contact-resonance frequencies. The values of k^* obtained in this manner represent the tip–sample contact stiffness. The elastic properties of the sample, namely the reduced modulus E^* and the indentation modulus M, can then be determined from the values of k^*. The exact relationship between k^* and M depends on the model for the tip–sample contact mechanics that is assumed [8]. The interpretation of AFAM results to obtain quantitative modulus values has been discussed in detail elsewhere [1,5]. In this paper, we are concerned with the effects of surface energy and humidity on

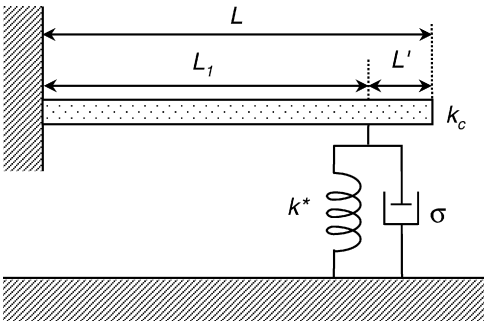

Fig. 1. Elements of the dynamic model for AFAM data analysis. The tip is located at a distance L_1 from the clamped end of the cantilever and a distance L' from the free end. The elastic and viscoelastic damping components of the tip–sample interaction are represented by a spring of stiffness k^* (contact stiffness) and a dashpot with characteristic damping σ, respectively.

the contact stiffness. Therefore, the interpretation of k^* to obtain modulus values is not discussed.

2.2. Preparation of SAM samples

The samples used in this study consisted of single-crystal (001) silicon (Si) substrates functionalized with self-assembled monolayers (SAMs) of *n*-octyldimethylchlorosilane (ODS). A detailed description of our fabrication methods has been given elsewhere [3,4,9]. Here, we briefly describe the two types of specimens fabricated for this study: unpatterned specimens with reference fields and graded micropattern specimens.

The first set of specimens, illustrated in Fig. 2, consisted of a SAM functionalized area adjacent to an unfunctionalized (bare Si) ''reference field.'' These samples were produced by masking half of the SiO_2-terminated Si substrate with a slab of polydimethylsiloxane (PDMS). Several of these slab/substrate systems were placed in a small vacuum desiccator along with a shallow boat containing $\sim$0.5 ml of ODS. A low vacuum in the desiccator helped to saturate the chamber with ODS vapor. The chlorosilane vapor reacted with those areas of the Si substrates that were not physically masked by the slabs. After a vapor exposure of 1 h, the specimens were removed from the desiccator and the stamps were peeled away. The substrates were then rinsed thoroughly with toluene and dried with dry nitrogen.

To produce specimens with various surface energies, the SAM-functionalized substrates were treated with ultraviolet-ozonolysis (UVO). In this process, UV radiation (wavelengths $\lambda = 184.9$ nm and 253.7 nm) creates ozone and atomic oxygen. This imparts the SAM with oxygen-containing moieties (primarily carboxylic acid groups) that raise the surface energy of the monolayer [4]. The surface energy γ thus increases according to the UVO exposure time. For example, representative ODS SAMs with no exposure to UVO are hydrophobic and exhibit $\gamma \approx 20$ mJ/m^2 and a water contact angle θ in the range of 90–95°. In contrast, for exposure times of about 70 s, the SAM is more hydrophilic, with $\gamma \approx 65$ mJ/m^2 and $\theta \approx 30°$. In this study, we employed a sample with no UVO exposure (measured $\theta = 90 \pm 2°$), and a specimen treated to 60 s of UVO exposure (measured $\theta = 45 \pm 2°$). In the discussion below, the unexposed SAM is referred to as the ''hydrophobic'' or ''ODS'' SAM, while the SAM exposed to UVO radiation is called the ''hydrophilic'' or ''ODS+UV'' SAM.

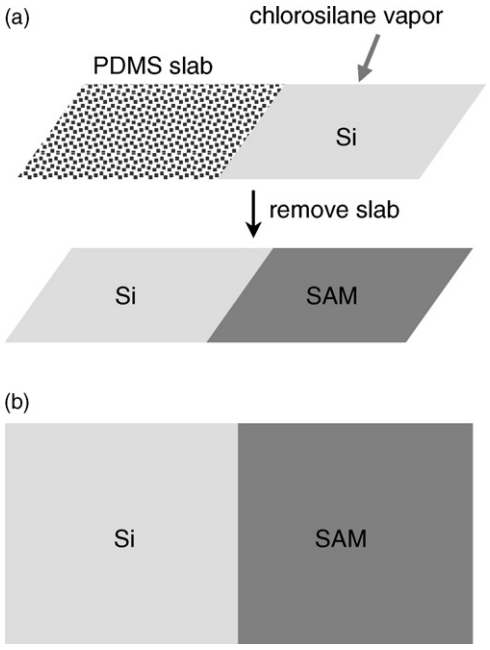

Fig. 2. ''Single-step'' SAM samples. (a) Samples were prepared by masking half of the Si substrate with a slab of polydimethylsiloxane (PDMS) and exposing it to chlorosilane vapor. After removal of the slab, the surface energy of the SAM could be altered by ultraviolet-ozone exposure if desired. (b) The resulting sample contained a SAM-functionalized area adjacent to a region of bare (oxide-terminated) Si.

The second type of specimen, illustrated in Fig. 3, had a micropatterned SAM that also exhibits a surface energy gradient. This ''combinatorial'' sample is designed to express a wide range of surface chemistries on a single substrate [9]. As shown in Fig. 3, fabrication of the specimen relies on a PDMS stamp patterned with series of ridges approximately 800 nm deep and 1.5 μm wide, with a pitch of 10 μm. When the corrugated PDMS stamp is applied to the substrate, it physically masks micrometer-sized strips of the Si surface. During SAM deposition, the ODS vapor traversed the microchannels formed by the edge-exposed stamp corrugations and the substrate, thus forming a SAM layer with a ''striped'' micropattern. To create the surface energy gradient, the patterned specimen is treated to a graded UVO exposure. This was accomplished via a custom-built device that employs a motorized stage to translate the substrate beneath a 2 mm wide aperture through which the UV source was transmitted [4,9]. By accelerating the stage, we create a SAM micropattern that gradually changes in its hydrophobicity. By design, this graded specimen includes interdigitated stripes of unfunctionalized Si, which serve as a static γ reference. Typical ranges of γ expressed by this combinatorial specimen are similar to those discussed above for unpatterned specimens.

SAMs produced by this or any other process will eventually degrade if exposed to environmental conditions such as high humidity or temperature. SAM lifetime can be significantly extended by proper specimen handling and storage. We have found that if samples are stored in a dark, cool desiccator, no measurable change in surface properties (i.e., in θ) can be detected for periods of 2 weeks or more. Nonetheless, measurements should be made as soon as possible after sample preparation. In this work, the AFAM measurements were performed on the samples less than 1 week after specimen fabrication.

2.3. RH experiments

The SAM samples described above provided an ideal system with which to examine the effect of surface energy on the measured contact stiffness. To broaden the scope of our study,

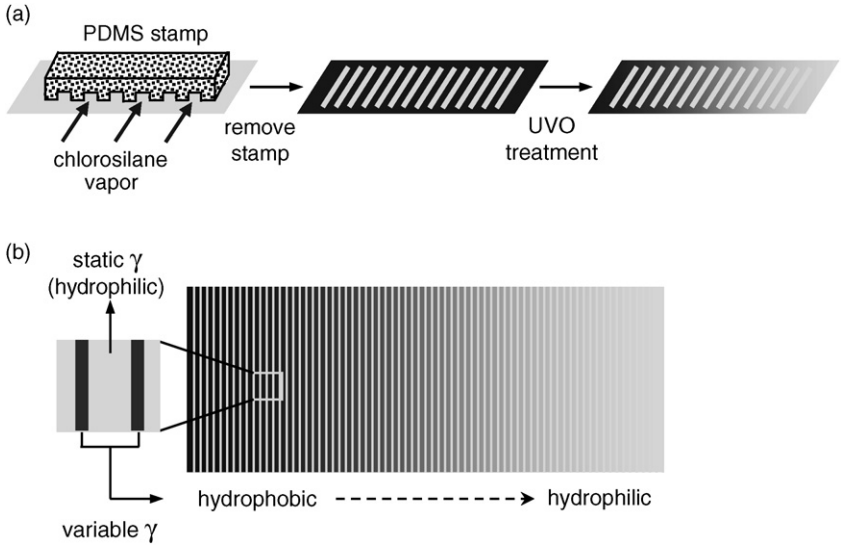

Fig. 3. Graded micropatterned SAM samples. (a) Samples were prepared by masking the sample with a patterned PDMS stamp and exposing it to chlorosilane vapor. After removal of the stamp, the sample was treated to a graded ultraviolet-ozone (UVO) exposure. (b) The resulting sample contained a series of SAM "stripes" whose surface energy systematically ranged from hydrophobic to hydrophilic, interspersed with regions of relatively hydrophilic oxide-terminated Si.

we also examined the influence of relative humidity. A relative humidity chamber was constructed for the AFM so that the ambient humidity could be systematically varied. The home-made RH chamber was fabricated from clear plastic and surrounded the entire AFM head assembly, the sample, and the sample positioning stage. Input ports were used to introduce dry and/or wet air into the chamber. Wet air was obtained by forcing compressed air through a beaker of distilled water. Dry air was created by forcing the compressed air through a beaker containing a commercial desiccant material. The relative amount of wet or dry air to compressed air, and hence the relative humidity in the chamber, was controlled by a manually adjusted mixing valve. The RH value in the chamber was monitored with a commercial RH meter having an operating range from 5% to 95% RH with an uncertainty of $\pm 1.5\%$. With these simple methods, we found that we could obtain RH values in the chamber that ranged between approximately 5% and 60% and that remained constant to within $\pm 2\%$ during the data acquisition period.

Qualitative AFAM amplitude images of the micropatterned SAM/Si sample were acquired at eight different sample locations that spanned the range of surface conditions from most hydrophobic to most hydrophilic. In these experiments, the humidity in the AFM chamber was first set as low as possible ($\sim 5\%$ RH). A single rectangular-shaped Si cantilever with spring constant $k_c \approx 40$ N/m was used to obtain all of the qualitative images. At each sample position, AFAM amplitude images were acquired using several (two to five) different excitation frequencies that differed by only a few kilohertz (e.g., 757 kHz, 759 kHz, and 762 kHz). By acquiring images at several frequencies, we could observe changes in the image contrast that provided qualitative information about the relative elastic properties of the SAM and silicon. The values of the contact-resonance frequencies (and thus the appropriate excitation frequency range) gradually increased over time due to wear of the AFM tip during scanning. Because we used a tip that was already worn, wear during these measurements was minimal and the increase in the contact-resonance frequencies was only a few kilohertz. After images were acquired at each of the eight positions, the humidity was increased to approximately 42% RH. AFAM amplitude images at several excitation frequencies for each position were again acquired. The positioning stages of the AFM made it possible to return to the same sample positions within a few micrometers.

Relative humidity experiments involving quantitative point measurements were performed separately on the hydrophobic and hydrophilic single-edge SAM samples. For each sample, the chamber humidity was set to the minimum value of 5% RH and a series of measurements was performed. A single rectangular Si cantilever with $k_c \approx 30$ N/m was used for all of the quantitative point measurements. (Prior to making the measurements, the cantilever was used repeatedly in scanning experiments in order to wear down the tip somewhat. We have found that this procedure minimizes tip wear during the measurements of interest and yields more consistent AFAM contact-resonance spectra.) Measurements were typically made at four slightly different sample positions at each RH value. For each sample position, AFAM spectra were acquired at three different cantilever deflections $\delta = 15$ nm, 30 nm, and 45 nm. Given the relation $F_c = k_c\delta$ between the deflection δ and the applied static load F_c, this implies that F_c ranged from approximately 0.45 μN to 1.35 μN in these experiments. In the results described below, data points for each RH value represent the average and standard deviation of 12 separate AFAM measurements (four positions with three values of F_c per position). After this set of measurements was completed, the humidity was incrementally increased and the measurement sequence was repeated until the maximum humidity was reached. Measurements were made initially at 5% RH and then at increments of 10% between 10% and 60% RH, for a total of seven different RH values.

3. Results and discussion

3.1. Qualitative images of humidity and surface-energy effects

Figs. 4 and 5 contain topography and AFAM amplitude images for two regions of the micropatterned SAM sample: a hydrophobic area (Fig. 4) and a hydrophilic area (Fig. 5). The topography (height) images, shown in Figs. 4(a) and 5(a), were acquired in contact mode simultaneously with the AFAM images. Two SAM stripes can be seen in each image. The z scale in both topography images is 5 nm, indicating that the thickness of the SAM stripes was 2–3 nm. In Fig. 5(a), the edges of the stripes are brighter (higher), and bright spots inside the SAM stripes are present. We believe these features represent some kind of contamination, possibly from the PDMS stamp. We omit consideration of these features in the discussion that follows.

AFAM amplitude images of the hydrophobic region of the sample acquired at approximately 5% and 42% RH are shown in Fig. 4(b) and (c), respectively. The corresponding AFAM images for the hydrophilic sample region are shown in Fig. 5(b, 5% RH and c, 42% RH). Each 512×128-pixel image took approximately 10 min to acquire. We estimated the surface energy γ and the wetting angle θ of the SAM in each region using reference curves obtained from measurements on other samples prepared in the same way. For the hydrophobic region, $\gamma \approx 35$ mJ/m^2 and $\theta \approx 80°$. For the hydrophilic region, $\gamma \approx 60$ mJ/m^2 and $\theta \approx 30°$. For the bare SiO_2-terminated Si substrate across the entire sample, $\gamma \approx 20$ mJ/m^2 and $\theta \approx 25°$.

One can quickly conclude from Figs. 4 and 5 that AFAM images provide much greater contrast (i.e., increased sensitivity) to the presence of the SAM than the topography images. More importantly, the figures also show that AFAM image contrast is affected by the surface energy of the sample and/or the ambient humidity. This fact can be understood by considering the figures separately. (Remember that images at several different excitation frequencies were acquired for each sample position and RH value. Comparison of the multiple images provided evidence for our conclusions.) There is little difference in contrast between the images in Fig. 4(b) and (c) acquired at 5% and 42% RH for the hydrophobic region of the SAM. Thus, the contact conditions between the tip and the hydrophobic SAM are not significantly affected by relative humidity. On the other hand, Fig. 5 reveals that the image contrast for the *hydrophilic* region of the SAM *does* change with relative humidity. In Fig. 5(b) for 5% RH, the Si regions appear brighter, while in Fig. 5(c) for 42% RH, the SAM stripes appear brighter. This inversion or reversal in image contrast with increasing humidity indicates that for the hydrophilic region of the SAM, the tip–sample contact conditions are significantly affected by relative humidity.

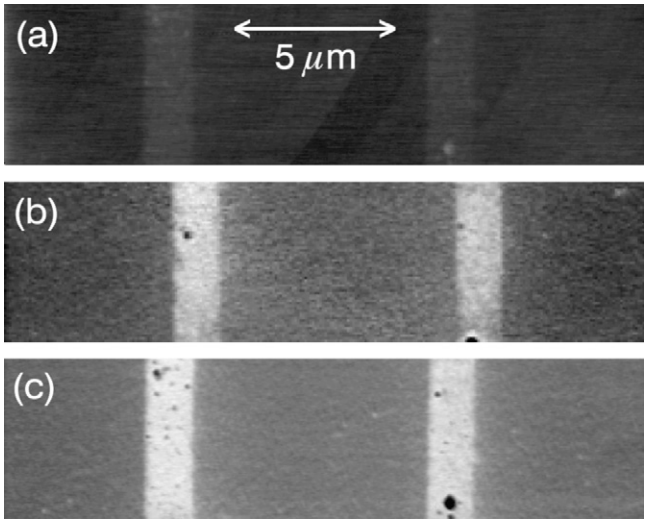

Fig. 4. Images of a hydrophobic ($\theta \approx 80°$) region of the micropatterned, graded-surface-energy SAM sample. (a) Topography. The full scale in z is 5 nm. (b) and (c) AFAM qualitative images of the same sample region at 5% and 42% RH, respectively.

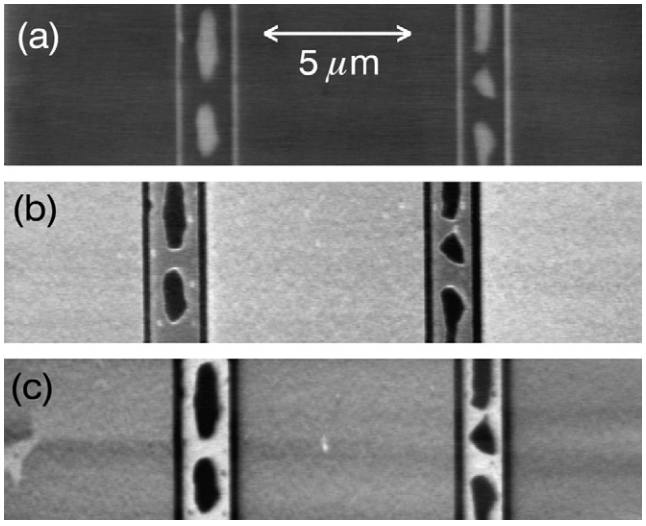

Fig. 5. Images of a hydrophilic ($\theta \approx 30°$) region of the micropatterned, surface-energy-gradient SAM on Si sample. (a) Topography. The full scale in z is 5 nm. The bright edges and irregular spots inside the SAM stripes are thought to correspond to contamination and should be disregarded. (b) and (c) AFAM qualitative images of approximately the same sample region at 5% and 42% RH, respectively.

In the AFAM images in Fig. 4, bright areas correspond to regions with lower contact-resonance frequencies. For a purely elastic tip–sample interaction (damping term $\sigma = 0$ in Fig. 1), higher contact-resonance frequencies correspond to elastically stiffer regions. Therefore, the hydrophobic SAM stripes appear more compliant than the Si substrate independent of relative humidity. In Fig. 5, however, bright areas correspond to regions with higher contact-resonance frequencies. Thus, the hydrophilic SAM stripes appear to be more compliant than the Si substrate at low humidities, but stiffer than the Si substrate at higher humidities.

It is difficult to draw further conclusions from the AFAM amplitude images without additional information about the contact-resonance frequencies. This information can be obtained from quantitative point measurements of contact-resonance spectra, which are discussed below. Nonetheless, imaging provides a rapid way to detect general trends in behavior. The images provide the first indication that the

tip–sample contact conditions depend on both surface energy and relative humidity. Furthermore, they give the first signal that care is needed for the correct interpretation of data obtained by AFAM—or indeed, by any nanoscale contact method conducted in ambient atmosphere rather than in vacuum.

3.2. Quantitative measurements of humidity and surface-energy behavior

The qualitative images in Figs. 4 and 5 show that the apparent tip–sample contact stiffness can be affected by both the surface energy and the relative humidity. To understand this effect in more detail, we measured the AFAM contact-resonance frequencies on the hydrophobic and hydrophilic single-step SAM samples as a function of relative humidity. The results are presented in Fig. 6. As discussed below, Fig. 6(a) shows the values of the contact stiffness k^* calculated assuming a purely elastic tip–sample interaction, while Fig. 6(b) shows the same data analyzed with an elastic–viscoelastic model.

The results in Fig. 6(a) were obtained using the elastic model shown in the figure inset, namely damping term $\sigma = 0$. To date,

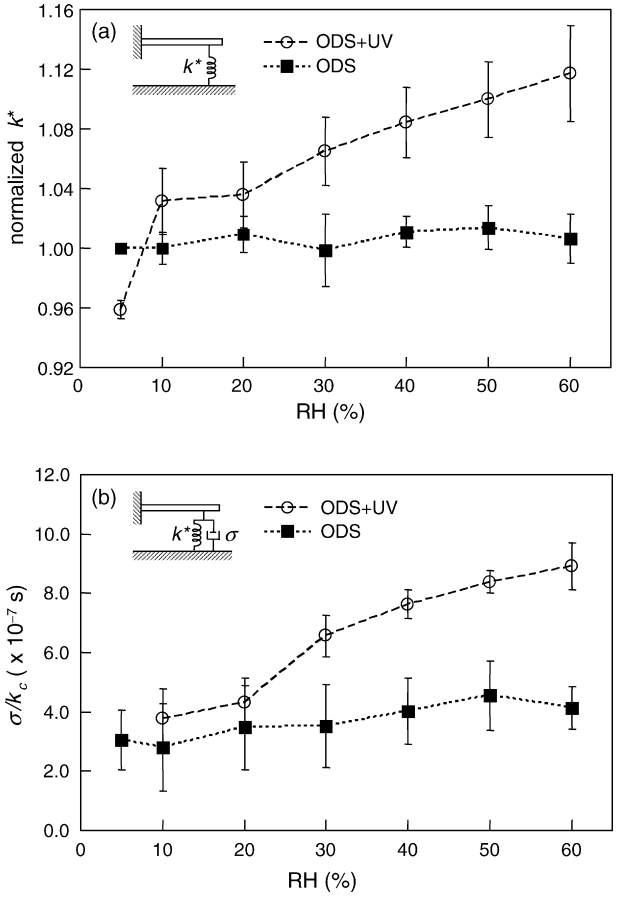

Fig. 6. Analysis of AFAM contact-resonance-frequency data as a function of relative humidity (RH) for the unexposed ODS (hydrophobic) and ODS+UV (hydrophilic) SAMs. The inset in each graph indicates the model used for the tip–sample interaction. (a) Apparent contact stiffness k^* assuming a purely elastic interaction. All of the values of k^* have been normalized to their values at 5% RH for the ODS SAM. (b) Damping term σ normalized by the cantilever spring constant k_c assuming an elastic–viscoelastic interaction. The values of σ/k_c were obtained assuming that k^* is independent of humidity.

virtually all AFAM measurements have been interpreted with this model. In Fig. 6(a), all of the values of k^* have been normalized to the average values of k^* at 5% RH for the hydrophobic (unexposed ODS) SAM. This normalization makes it possible to combine all of the results at each RH value regardless of the applied static load F_c. The error bars in the figure correspond to the standard deviation in 12 measured values of k^*. The graph shows that for the hydrophobic ODS SAM, k^* remains constant within measurement uncertainty for all values of relative humidity. This behavior is consistent with that observed in the qualitative images in Fig. 4(b) and (c). In contrast, the calculated values of k^* for the hydrophilic ODS+UV SAM increase monotonically with RH. At about 5–10% RH, the average values of k^* are approximately the same as those for the ODS SAM; at 60% RH, k^* is greater by $\sim 12\%$.

The true contact stiffness represents an elastic tip–sample interaction; therefore, it should not depend on the ambient humidity. Because the SAM is so thin (~ 2–3 nm), we argue that AFAM measurements are not sensitive to the elastic properties of the SAM, but reflect the elastic properties of the underlying Si substrate only. Thus, the true value of k^* should remain constant with relative humidity. We believe that the increase in k^* with RH observed for the ODS+UV SAM sample results from the use of an overly simplistic analysis model. A more complex model for the tip–sample interaction is needed to realistically model the system for accurate data interpretation. Physically, we attribute the apparent increase in k^* with RH to a humidity-dependent capillary bridge or meniscus between the tip and the sample formed by the ODS+UV SAM. Capillary effects can be modeled by the inclusion of a viscoelastic damping term ($\sigma \neq 0$ in Fig. 1). If capillary forces are not explicitly included in the analysis model, the net effect is an apparent increase in the contact radius a with RH. Because $k^* = a/2E^*$ for axisymmetric tip shapes [8], the apparent increase in a with RH will manifest itself as an apparent increase in k^*. This is our explanation for the behavior of k^* in Fig. 6(a).

We therefore re-analyzed the AFAM data with a model that included both elastic and viscoelastic terms. The analysis approach has been described previously [2]. First, a constant value k_0^* of the contact stiffness was chosen. There are several possible ways to choose the value of k_0^*. Here, we used the values obtained by fitting each set of data in Fig. 6(a) to a straight line. The y-intercept of each line, that is, k^* for 0% RH, was used as the value of k_0^*. Each datum was then analyzed to find the value of σ for which the measured contact-resonance frequencies corresponded to that value of k_0^*. Fig. 6(b) shows the results of this analysis. The graph contains the calculated values of the quantity σ/k_c (damping term normalized by the cantilever spring constant). If $k_c = 30$ N/m is assumed for the cantilever used here, the range of the y-axis in Fig. 6(b) corresponds to $\sigma = 360 \times 10^{-7}$ kg/s. The points represent the average measured values, while the error bars indicate the standard deviation in individual measurements at each RH value for each sample. The graph shows that for the hydrophobic ODS sample, σ/k_c is the same within measurement uncertainty for all values of RH. This behavior is not surprising, based on Fig. 6(a). The average

value of the normalized damping term for the ODS sample is $\sigma_{ODS}/k_c = 2.2 \pm 0.3 \times 10^{-7}$ s. It appears that σ/k_c may increase slightly as the humidity increases, but the measurement uncertainties are too large to state this for certain.

More importantly, Fig. 6(b) shows that the damping term for the hydrophilic ODS+UV SAM systematically increases with humidity. (There is no data point for 5% RH because all of the measured values of k^* were less than the assumed value k_0^*.) At low RH values, the damping values are the same within the uncertainty as the values for the ODS SAM. At approximately 20–30% RH, a transition point occurs at which σ/k_c increases significantly. The increase is more gradual for RH values higher than the transition value. Overall, σ/k_c increases by a factor of approximately 2.5 from 10% to 60% RH. The increase in σ is consistent with our hypothesis of capillary forces that increase with humidity.

The observed behavior is also consistent with previous work on the humidity dependence of tip–sample capillary forces [10–13]. These studies examined tip–sample capillary forces by measuring AFM pull-off forces as a function of relative humidity on various materials. The findings were similar for each case. Pull-off forces remained relatively low and approximately constant with RH for hydrophobic materials such as a SAM of *n*-octadecyltrimethoxysilane, but increased with RH for hydrophilic samples such as oxide-terminated Si [10]. In each case, a transition point occurred in the range from about 20% to 50% RH depending on the sample surface energy and other experimental conditions [11]. Analytical expressions were developed that related the humidity dependence of the pull-off force to parameters such as the surface energy and the tip radius [11,12].

Typical values of the measured pull-off forces in these studies were approximately 10–100 nN. In order to achieve deflection sensitivity in this force range, cantilevers with stiffness k_c approximately 0.1–0.5 N/m were used. Our AFAM experiments used much stiffer cantilevers (stiffness approximately 30–40 N/m). Therefore, they have little sensitivity to variations in pull-off forces of this magnitude, and a direct comparison between the AFAM results and the pull-off forces cannot be made. Despite the difference in experimental approach, the similarity in behavior between the AFAM damping term and the pull-off forces strongly suggests that the two effects are related in some way. Further research is needed to elucidate the quantitative link between the cantilever vibrational model (the dashpot in Fig. 1) and physical properties such as the surface energy.

4. Summary and conclusions

We have investigated the effects of surface functionality and relative humidity on nanoscale contact stiffness. Our samples contained micropatterned and blanket ODS SAMs. By varying the length of exposure to UV-ozone radiation, the surface energy of the SAMs could be varied from hydrophobic to hydrophilic. Qualitative AFAM amplitude images of a micropatterned, surface-energy-gradient SAM sample showed higher contrast between the SAM and the Si substrate than could be achieved from topographic imaging. The images also revealed that image contrast depended on both the relative humidity and the surface energy of the SAM.

These effects were examined systematically with quantitative AFAM point measurements of the contact-resonance frequencies on hydrophobic and hydrophilic SAMs under controlled humidity conditions. When the cantilever dynamics were analyzed by assuming solely elastic interaction forces, the calculated contact stiffness k^* remained roughly constant with RH for the hydrophobic ODS SAM. However, the apparent contact stiffness increased with relative humidity for the hydrophilic ODS+UV SAM. A viscoelastic damping term was added to the data analysis model to account for capillary forces created by the SAM. To obtain a constant value of k^* on the hydrophilic SAM, the normalized damping term σ/k_c increased significantly with RH with a transition point between 20% and 30% RH. The observed RH behavior of the damping was very similar to the behavior of AFM pull-off forces reported by other groups.

These results indicate that surface and environmental conditions can influence measurements of nanomechanical properties with AFM methods such as AFAM. Our work illustrates why sufficient information about sample properties (e.g., surface energy) and operating conditions (e.g., relative humidity) is necessary to obtain accurate measurement results. We plan to continue AFAM experiments on a variety of materials under different conditions. In this way, we may better understand the complex interplay between different physical parameters and their impact on quantitative measurements of nanomechanical properties.

Acknowledgements

Paul Rice (NIST and University of Colorado-Boulder) designed the relative humidity chamber and assisted with its implementation. We thank Joseph Turner (University of Nebraska-Lincoln) and Ute Rabe and Walter Arnold (Fraunhofer Institute for Nondestructive Testing, Germany) for valuable discussions.

References

[1] U. Rabe, S. Amelio, E. Kester, V. Scherer, S. Hirsekorn, W. Arnold, Quantitative determination of contact stiffness using atomic force acoustic microscopy, Ultrasonics 38 (2000) 430–437.
[2] D.C. Hurley, J.A. Turner, Humidity effects on the determination of elastic properties by atomic force acoustic microscopy, J. Appl. Phys. 95 (2004) 2403–2407.
[3] A. Sehgal, A. Karim, C.M. Stafford, M.J. Fasolka, Techniques for combinatorial and high-throughput microscopy. Part I: Gradient specimen fabrication for polymer thin film research, Microsc. Today 11 (September) (2003) 26–30.
[4] S.V. Roberson, A.J. Fahey, A. Sehgal, A. Karim, Multifunctional ToF-SIMS: combinatorial mapping of gradient energy substrates, Appl. Surf. Sci. 200 (2002) 150–164.
[5] D.C. Hurley, K. Shen, N.M. Jennett, J.A. Turner, Atomic force acoustic microscopy methods to determine thin-film elastic properties, J. Appl. Phys. 94 (2003) 2347–2354.
[6] U. Rabe, S. Amelio, M. Kopycinska, S. Hirsekorn, M. Kempf, M. Göken, W. Arnold, Imaging and measurement of local mechanical properties by

atomic force acoustic microscopy, Surf. Interface Anal. 33 (2002) 65–70.
[7] U. Rabe, J.A. Turner, W. Arnold, Analysis of the high-frequency response of atomic force microscope cantilevers, Appl. Phys. A 66 (1998) S277–S282.
[8] K.L. Johnson, Contact Mechanics, Cambridge University Press, Cambridge, UK, 1985.
[9] D. Julthongpiput, M.J. Fasolka, W. Zhang, T. Nguyen, E.J. Amis, Gradient chemical micropatterns: a reference substrate for surface nanometrology, Nano Lett. 5 (2005) 1535–1540.
[10] X. Xiao, L. Qian, Investigation of humidity-dependent capillary force, Langmuir 16 (2000) 8153–8158.
[11] D.L. Sedin, K.L. Rowlen, Adhesion forces measured by atomic force microscopy in humid air, Anal. Chem. 72 (2000) 2183–2189.
[12] T. Thundat, X.-Y. Zheng, Y. Chen, R.J. Warmack, Role of relative humidity in atomic force microscopy imaging, Surf. Sci. Lett. 294 (1993) L939–L943.
[13] T. Nguyen, X. Gu, L. Chen, D. Julthongpiput, M. Fasolka, K. Briggman, J. Hwang, J. Martin, Effects of surface functionality and humidity on the adhesion force and chemical contrast measured with AFM, in: S.V. Kalinin, B. Goldberg, L.M. Eng, B.D. Huey (Eds.), Scanning-Probe and Other Novel Microscopies of Local Phenomena in Nanostructured Materials—Mater. Res. Soc. Symp. Proc. 838E, Warrendale, PA, 2005, O15–5.